

ScN/GaN(1 $\bar{1}$ 00): a new platform for the epitaxy of twin-free metal-semiconductor heterostructures

P. John,* A. Trampert, D.-V. Dinh, D. Spallek, J. Lähnemann, V. Kaganer,
L. Geelhaar, O. Brandt, and T. Auzelle

*Paul-Drude-Institut für Festkörperelektronik, Leibniz-Institut im Forschungsverbund Berlin e.V.,
Hausvogteiplatz 5-7, 10117 Berlin*

E-mail: john@pdi-berlin.de

Abstract

We study the molecular beam epitaxy of rock-salt ScN on the wurtzite GaN(1 $\bar{1}$ 00) surface. To this end, ScN is grown on free-standing GaN(1 $\bar{1}$ 00) substrates and self-assembled GaN nanowires that exhibit (1 $\bar{1}$ 00) sidewalls. On both substrates, ScN crystallizes twin-free thanks to a specific epitaxial relationship, namely ScN(110)[001]||GaN(1 $\bar{1}$ 00)[0001], providing a congruent, low-symmetry GaN/ScN interface. The 13.1% uniaxial lattice mismatch occurring in this orientation mostly relaxes within the first few monolayers of growth by forming a coincidence site lattice, where 7 GaN planes coincide with 8 ScN planes, leaving the ScN surface nearly free of extended defects. Overgrowth of the ScN with GaN leads to a kinetic stabilization of the zinc blende phase, that rapidly develops wurtzite inclusions nucleating on {111} nanofacets, commonly observed during zinc blende GaN growth. Our ScN/GaN(1 $\bar{1}$ 00) platform opens a new route for the epitaxy of twin-free metal-semiconductor heterostructures made of closely lattice-matched GaN, ScN, HfN and ZrN compounds.

Keywords

GaN/ScN heterostructures, core/shell nanowires, twin-free epitaxy, transition metal nitrides, metal-semiconductor heterostructures, uniaxial strain

To enhance the functionalities of conventional group III_A-nitride (III_A-N) devices that are based on the semiconductors AlN, GaN or InN, combinations with transition metal nitrides (TMNs) like NbN, ScN, ZrN or TiN are sought.¹⁻³ These “new nitrides” bring in distinctive properties such as superconductivity,² ferroelectricity,⁴ catalytic activity⁵ or plasmonic resonances in the visible spectrum.^{6,7} This opens up new prospects for enhancing the performance of current devices or creating innovative new ones. To fully realize this potential, successful heterostructuring of the TMNs with III_A-N semiconductors will necessitate epitaxial integration with a low density of extended defects. However, while the hexagonal wurtzite phase is the most stable one for III_A-nitrides, the cubic rock-salt structure is the common phase for TMNs. Due to the different crystal symmetry, rotational twins are inevitable for the growth of TMNs on the (0001) plane of hexagonal GaN, SiC, or Al₂O₃⁸ — the substrates most commonly used for III_A-N heterostructures and devices. Twin domain boundaries locally reduce the crystal symmetry and may thus exhibit dramatically different properties compared to the bulk. In the context of opto-electronic devices, remarkable examples are superconducting twin boundaries in otherwise insulating WO_x (with $x \approx 3$), or twin boundaries hosting polarization singularities in otherwise nonpolar perovskite structures.⁹ Concerning TMNs,

preliminary observations suggest that twin boundaries in NbN are not superconducting, which will lower the overall critical temperature of the material.¹⁰

To achieve single-domain TMN layers on hexagonal GaN substrates, we investigate here the epitaxy of ScN on the $(1\bar{1}00)$ surface (also referred to as *M*-plane surface), since it has a lower symmetry than the conventional (0001) surface (also referred to as *C*-plane surface). $(1\bar{1}00)$ facets are of practical relevance as they can be realized on large substrates (≥ 2 inches) either dislocation-free on the sidewalls of most GaN micro- and nanostructures prepared top-down and bottom-up,^{11–14} or with dislocations by heteroepitaxy on γ -LiAlO₂ substrates.^{15,16} Here, ScN is merely used as a model system because it can be grown lattice-matched to GaN^{3,17,18} and, unlike most transition metals, Sc can be evaporated using an effusion cell. We find that ScN grows free of twins on GaN $(1\bar{1}00)$ thanks to a specific epitaxial relationship. We obtain this finding by growing twin-free ScN both on free-standing GaN $(1\bar{1}00)$ substrates and self-assembled GaN nanowires. These

two types of substrates facilitate the use of different analytical techniques, yielding consistent results. The uniaxial strain occurring in ScN/GaN $(1\bar{1}00)$ is relaxed via a coincidence site lattice, making the ScN layers suitable for regrowth of twin-free cubic nitrides.

ScN is first grown by plasma-assisted molecular beam epitaxy (PAMBE) on self-assembled GaN nanowires (NWs) under N-rich conditions to impede the formation of N-vacancies.^{19,20} Representative secondary electron micrographs of a GaN NW before and after ScN growth are displayed in Figures 1(a) and 1(b), respectively. ScN deposited on the $(000\bar{1})$ NW top-facet forms a cubic crystallite, whereas ScN grown on the $(1\bar{1}00)$ NW sidewalls forms a relatively smooth layer. The ScN shell and cube exhibit different crystallographic orientations, which are related to their distinct epitaxial relationships with the underlying GaN facet. As schematized in Figure 1(e), the ScN cube follows the same epitaxial relationship as commonly found for ScN on GaN (0001) substrates, namely ScN $(111)[1\bar{1}0]||$ GaN $(000\bar{1})[11\bar{2}0]$.^{17,18,20} Twinning is observed between cubes located on

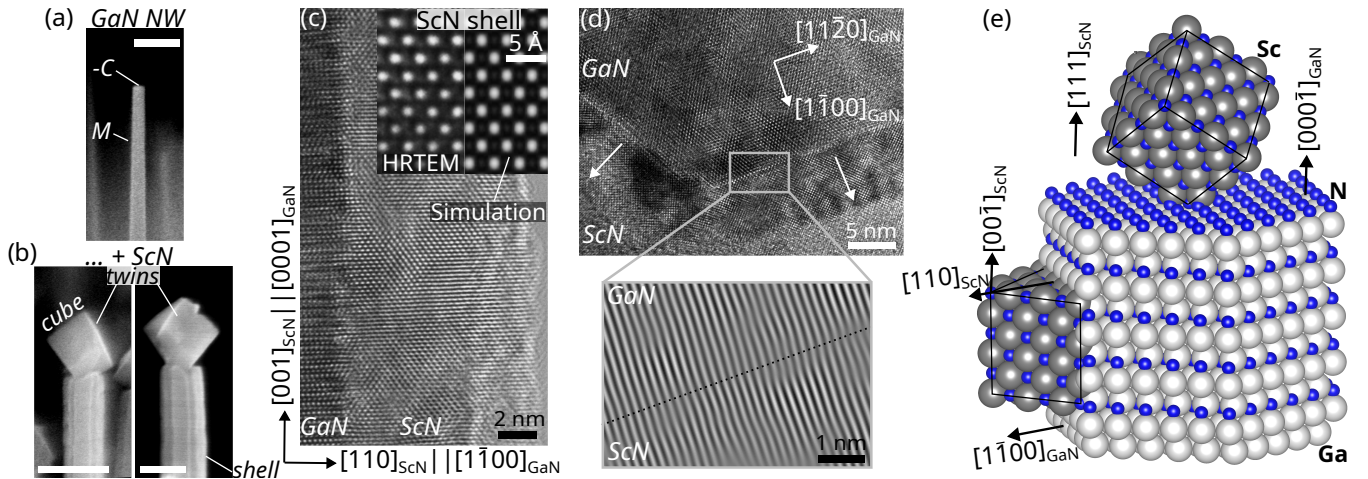


Figure 1: Secondary electron micrographs of GaN NWs (a) before and (b) after overgrowth with a 25 nm thick ScN shell. The scale bars indicate 200 nm. (c) HRTEM of the interface between the GaN core and a 10 nm thick ScN shell with $[11\bar{2}0]_{\text{GaN}}$ zone axis. The inset compares a magnified HRTEM image with a simulation using the epitaxial relationship described in the main text. (d) HRTEM along the NW axis, i.e., with $[0001]_{\text{GaN}}$ zone axis. White arrows within the ScN shell indicate ScN $[110]$ directions. An inverse Fourier-filtered section from the GaN/ScN interface, highlighting GaN $(11\bar{2}0)$ and ScN $(1\bar{1}0)$ planes, is shown in the bottom panel. (e) Schematic representation of the local GaN/ScN epitaxial relationships at the NW tip and sidewall.

different NWs or even within the same NW (the latter not shown here). In contrast, a very different epitaxial relationship is found for the ScN shell on the GaN NW sidewalls. Figure 1(c) shows a high-resolution transmission electron microscopy (HRTEM) image of the ScN shell taken with the zone axis parallel to the $[11\bar{2}0]_{\text{GaN}}$ direction. No twin domains are found after analyzing ≈ 10 NWs. Comparison with the simulation shown in the inset of Figure 1(c) reveals the orientation-relationship $\text{ScN}(110)[001]||\text{GaN}(1\bar{1}00)[0001]$. This finding is confirmed by plan-view HRTEM along the $[0001]_{\text{GaN}}$ zone axis. Figure 1(d) reveals a smooth ScN shell nucleating on well-defined $\text{GaN}\{1\bar{1}00\}$ facets. Since the GaN/ScN orientation-relationship holds on every facet of the NW core, the ScN nucleating on adjacent $\{1\bar{1}00\}_{\text{GaN}}$ facets is separated by high-angle boundaries, leading eventually to the formation of vertical grooves as observed in Figure 1(b). The orientation-relationship reported here has already been observed between ScN and AlN as a result of thermal decomposition of (Sc,Al)N thin films,²¹ but it is not systematic for all rock-salt compounds grown on wurtzite $(1\bar{1}00)$ planes (e.g., MgO on ZnO²²).

To confirm the epitaxial relationship and the twin-free nature of ScN on a large scale, a 40 nm-thick film is grown on a free-standing $\text{GaN}(1\bar{1}00)$ substrate. On such a reference surface, illustrated in the atomic force topograph of Figure 2(a), the ScN orientation is monitored *in situ* by reflection high-energy electron diffraction (RHEED). The patterns taken along the $[1\bar{1}0]_{\text{ScN}}$ and $[001]_{\text{ScN}}$ azimuths (Figures 2(c) and (d), respectively) perfectly match the ones simulated using the epitaxial relationship found for the NW shell and shown by black dots. The presence of 45° chevrons in the pattern along the $[001]_{\text{ScN}}$ azimuth indicates that the layer is terminated by $\{100\}$ facets.²³ In N-rich conditions, such $\{100\}$ facets are stoichiometric^{24,25} and are typically the ones of lowest energy in rock-salt compounds.²⁶ The nanofaceting of the ScN layer is confirmed by the atomic force topograph shown in Figure 2(b), evidencing

an anisotropic surface morphology consisting of periodic stripes, which are oriented along the $[001]_{\text{ScN}}$ direction. We attribute this anisotropic surface structure to an anisotropy in the adatom diffusion barriers along the ScN $[001]$ and $[1\bar{1}0]$ directions.

To confirm the absence of small inclusions with a different epitaxial relationship, the ScN film is probed at the μm scale with electron backscatter diffraction (EBSD). The pseudo-Kikuchi pattern exemplified in Figure 2(e) is composed of sharp bands, enabling fast and reliable indexing when mapping large areas. Figure 2(f) shows the resulting EBSD orientation map, confirming that the film is single crystalline. The tilt distribution is around 1° ,

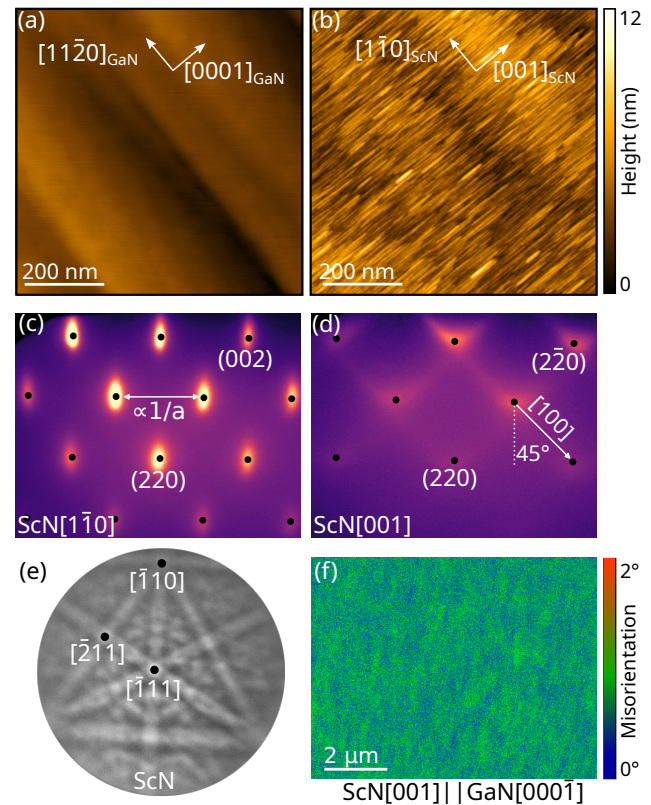


Figure 2: Atomic force topographs of (a) a free-standing $\text{GaN}(1\bar{1}00)$ substrate and (b) a 40 nm thick ScN layer. (c) and (d) RHEED patterns and superimposed diffraction simulations (black dots) along the ScN azimuths indicated in the bottom left corner. (e) EBSD pseudo-Kikuchi pattern and (f) in-plane orientation map of the ScN layer, where variations in color show the local deviation from the nominal ScN orientation indicated below.

close to the resolution limit of the technique.

Careful analysis of both the NW shells and the thin films indicates the absence of twin domains. This can be understood by looking at the atomic configuration of the ScN/GaN interface, schematized in Figure 3(a). For the experimentally determined epitaxial relationship, GaN and ScN are lattice-matched along the $[1\bar{1}20]_{\text{GaN}}$ direction, but display a 13.1% mismatch along the $[0001]_{\text{GaN}}$ direction. No other favorable atomic configuration can be found by rotating or mirroring the ScN lattice in the interfacial plane, and the mirror symmetry of GaN($1\bar{1}00$) matches the one of ScN(110), which are the two necessary conditions to achieve single-domain ScN layers.⁸ One competing epitaxial relationship, however, would be that observed for ScN deposited on GaN(0001) (*e.g.*, as seen for MgO on ZnO NWs²²). Indeed, for ScN on GaN($1\bar{1}00$), such a configuration would lead to a very low epitaxial strain ($< 0.5\%$), but the mismatch between the AB_{GaN} and ABC_{ScN} plane stacking sequence would most likely result in a much higher density of dangling bonds, as explained in the Supporting Information. There-

fore, the most favorable interfacial atomic configuration appears here to be the one that minimizes the number of dangling bonds, but with significant epitaxial strain.

The critical thickness for plastic relaxation of the huge uniaxial lattice mismatch (13.1%) imposed by the GaN substrate on the ScN layer is less than one monolayer (ML). We thus expect the ScN layer to quickly approach its strain-free lattice parameter taken as 4.505 \AA .²⁷ Consistently, Moiré patterns are observed during the TEM observations of GaN/ScN core/shell NWs [Figure 3(b)], resulting from the superposition of two lattices with different lattice parameters.²⁸ The Moiré period along the NW axis ($[001]_{\text{ScN}}$ direction) is $1.9 \pm 0.1 \text{ nm}$, which corresponds to a residual strain of $1.3 \pm 0.7\%$ for the 12 nm thick ScN shell.

Inverse Fourier filtering of an HRTEM image of the ScN/GaN interface is used to highlight the GaN(0002) and ScN(002) planes at the GaN/ScN interface. It evidences a regular array of misfit dislocations with a period of $7 d_{\text{GaN}}^{(0002)} = 8 d_{\text{ScN}}^{(002)} = 1.8 \text{ nm}$, as displayed in right panel in Figure 3(b), d indicating the respective inter-planar lattice distance. In con-

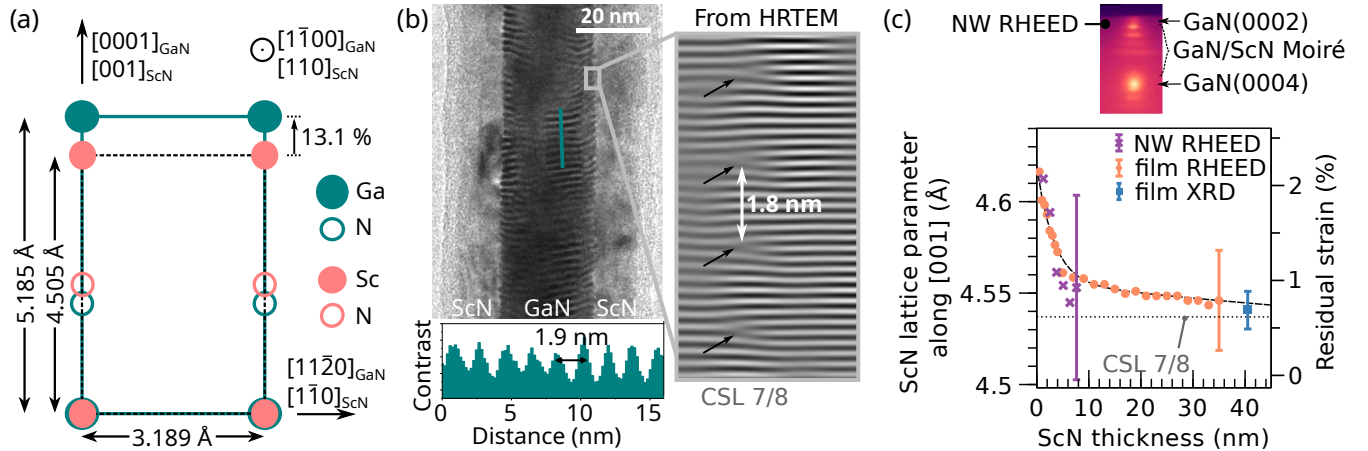


Figure 3: (a) Schematic atomic arrangement of two-dimensional ScN(110) and GaN($1\bar{1}00$) unit meshes. (b) TEM of a GaN/ScN core/shell NW along the $[1\bar{1}20]_{\text{GaN}}$ zone axis revealing Moiré patterns. An intensity profile taken along the green line is shown in the bottom panel, and an inverse Fourier-filtered section from a HRTEM image of the interface, highlighting GaN(0002) and ScN(002) planes, is shown in the right panel. Misfit dislocations are indicated by black arrows. (c) ScN lattice parameter measured in films and NWs with RHEED and XRD along the $[001]_{\text{ScN}}$ direction, as a function of layer thickness. The error bars represent the errors for all data points of the respective measurements. The top panel exemplifies a section of the RHEED pattern during GaN/ScN core/shell NW growth along the $[1\bar{1}00]_{\text{GaN}}$ azimuth.

trast, misfit dislocations are absent along the $[11\bar{2}0]_{\text{GaN}}$ direction [see bottom panel in Figure 1(d)], where the ScN lattice matches the one of GaN. The dislocations are thus of pure edge (90°) character and form a $7/8$ coincidence site lattice (CSL), for which a residual strain state of $\approx 0.6\%$ is expected. Similar arrays of pure edge dislocations are typically observed in highly-mismatched heterostructures,^{29–32} which do not necessarily lead to a large density of threading dislocations.³² Here, no obvious sign for threading dislocations nor stacking faults could be seen within the ≈ 10 NWs examined by TEM.

Next, we closely monitor the kinetics of the strain relaxation using RHEED.³³ In the thin film case, the ScN lattice parameter in the $[001]_{\text{ScN}}$ direction is directly retrieved from its reciprocal space lattice measured along the $[1\bar{1}0]_{\text{ScN}}$ azimuth [cf. Figure 2(c)] and taking $c_{\text{GaN}} = 5.185 \text{ \AA}$ for the initial GaN substrate.³⁴ In the NW case, satellites around the GaN Bragg peaks occur, as displayed in the top panel of Figure 3(c). These satellites are the result of the successive transmission of the electron beam through the NW core and shell, and can be seen as the Fourier transform of the core/shell GaN/ScN Moiré pattern with $p^* = a^* + c^*$, where p^* , a^* and c^* are the reciprocal lattice vectors of the Moiré pattern, ScN shell and GaN core, respectively, averaged over $\approx 10^7$ NWs.

The ScN lattice parameter and residual strain along its $[001]$ axis, extracted from the RHEED analysis of the film and the NWs, are displayed in Figure 3(c) as a function of the ScN thickness. For both layers and NWs, plastic relaxation is observed already at the onset of ScN growth. The strain of the first ScN monolayer is already reduced to $2.0 \pm 0.5\%$. Such immediate strain reduction could be explained by the formation of an $8/9$ CSL that releases a mismatch of 11.1% . For further ScN growth of up to 40 nm in thickness, strain decreases and tends to saturate at a minimum value of $\approx 0.7\%$, coinciding with the expected value for a CSL of $7/8$ lattice planes for GaN and ScN. This value is also confirmed by X-ray diffractometry (XRD) performed on the 40 nm

thick ScN film.

A further reduction of the CSL period down to $6/7$ lattice planes would overcompensate the mismatch, which does not decrease further the elastic strain energy of the ScN film. Complete strain relaxation therefore implies a break in the CSL periodicity, which is energetically unfavorable and thus explains the apparent saturation of the residual strain at a value of 0.7% for ScN film thicknesses above 10 nm. As a result, the top surface of the 40 nm-thick ScN layer grown on GaN($1\bar{1}00$) exhibits a uniaxial strain of $\approx 0.7\%$, but essentially no extended defects like twin-domain boundaries, stacking faults, or threading dislocations. This is particularly favorable for regrowth of cubic transition metal nitride heterostructures on GaN with high structural perfection.

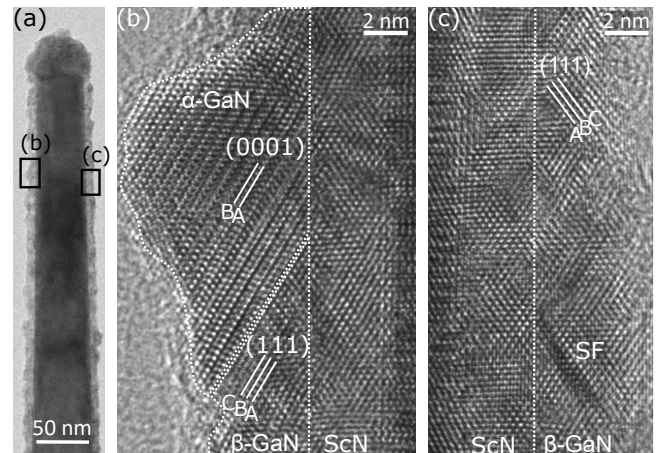


Figure 4: TEM of a GaN/ScN core/shell NW overgrown by GaN, along the $[11\bar{2}0]_{\text{GaN}}$ zone axis of the NW core. (a) Overview showing a rough NW shell. Magnified images in (b) and (c) reveal the presence of mixed α -GaN/ β -GaN and pure β -GaN domains, respectively.

An interesting question is whether the epitaxial relationship found for ScN grown on GaN($1\bar{1}00$) holds also when GaN is regrown on ScN. To clarify this point, GaN is first deposited on GaN/ScN core/shell NWs and representative TEM micrographs of the resulting GaN/ScN/GaN core/shell structure are shown in Figure 4. The 3 nm-thick GaN shell is rougher than the underlying ScN(110) surface and contains both wurtzite

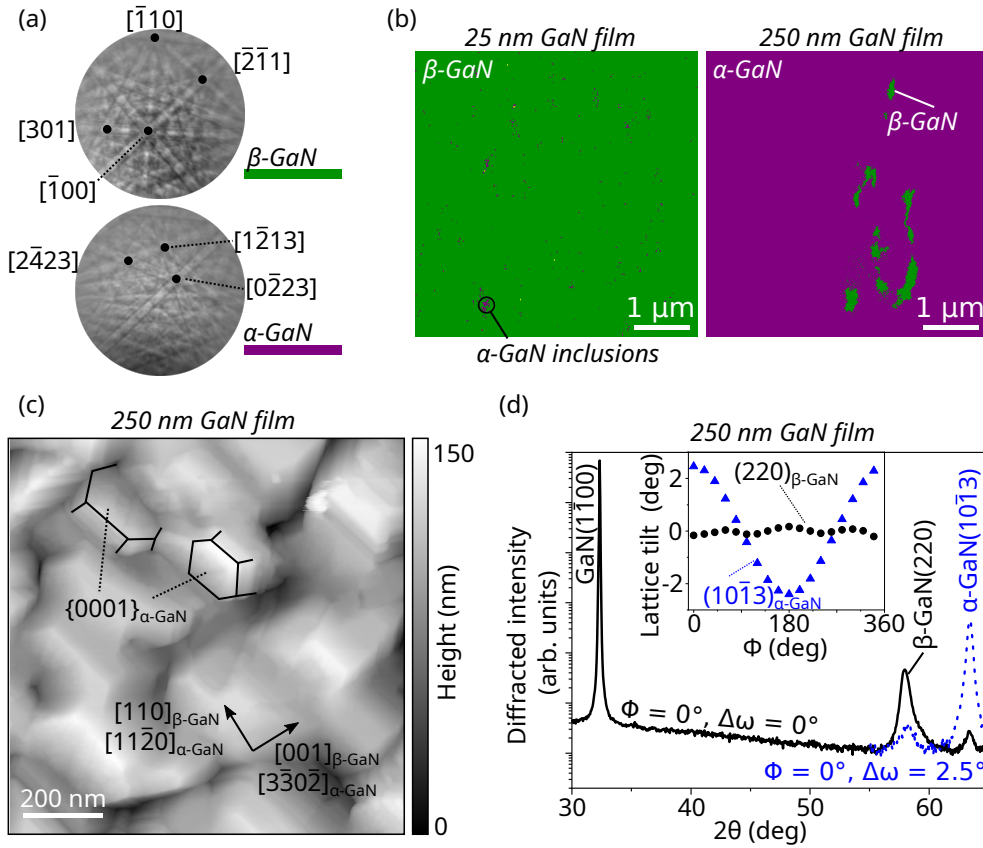


Figure 5: EBSD patterns (a) and phase maps (b) acquired on the 25 and 250 nm thick GaN layers grown on ScN(110)/GaN(1 $\bar{1}00$) heterostructures.

(c) Atomic force topograph of the 250 nm thick GaN layer. (d) XRD $2\theta/\omega$ scan of the same layer, revealing the presence of α -GaN and β -GaN, tilted relative to each other. The inset shows the lattice tilt of α -GaN and β -GaN as a function of azimuth ϕ , evidencing $\approx 2.5^\circ$ of α -GaN(10 $\bar{1}3$) relative to the substrate.

(α -GaN) and zinc blende (β -GaN) phases [Figure 4(b)]. The cubic β -GaN domains share the same orientation as the underlying ScN, namely β -GaN(110)[001] || ScN(110)[001], resulting in a perfectly commensurate interface [Figure 4(c)]. The low energy of the interface is certainly a key factor in explaining the kinetic stabilization of the otherwise thermodynamically unstable zinc blende phase. Surprisingly, the wurtzite crystal phase does not follow the epitaxial relationship found for ScN deposited on GaN(1 $\bar{1}00$). Instead, α -GaN inclusions nucleate on stacking faults (SFs) preferentially formed on $\{111\}_{\beta\text{-GaN}}$ facets, as commonly observed in rough β -GaN films.³⁵ The epitaxial relationship at the wurtzite - zinc blende interface is then given by α -GaN(0001)[11 $\bar{2}0$] || β -GaN(111)[1 $\bar{1}0$]. This translates into the effective orientation of α -GaN(1 $\bar{1}03$)[11 $\bar{2}0$] || ScN(110)[1 $\bar{1}0$] with the underlying ScN. The same orientation has been observed for α -GaN inclusions occurring during the growth of β -GaN on MgO(110)³⁶ and GaAs(110).^{37,38} Here, a 3.3° tilt between the α -GaN[1 $\bar{1}03$] and ScN[110] directions is

expected in the absence of strain.

Continued GaN growth leads to an increase in the size of the wurtzite inclusions, which eventually cover the entire surface. This is evidenced by growing 25 and 250 nm-thick GaN layers on ScN/GaN(1 $\bar{1}00$) films. EBSD patterns and phase maps of the two layers are displayed in Figures 5(a) and (b), respectively. The thinner GaN layer exhibits mostly the zinc blende phase, whereas the thicker one shows mostly the wurtzite phase. In spite of the metal-rich growth conditions, the atomic force topograph acquired on the thicker GaN layer and shown in Figure 5(c) reveals a faceted surface, most of them being attributed to wurtzite {0001} and {1 $\bar{1}00$ } facets, from which we conclude that α -GaN{1 $\bar{1}03$ } facets are unlikely to be stabilized. Two different in-plane α -GaN orientations are found, resulting from the nucleation on both (111) and (11 $\bar{1}$) facets of the initial β -GaN layer. A symmetric $2\theta/\omega$ XRD scan of the 250 nm GaN film is displayed in Figure 5(d). It evidences the presence of both β -GaN(220) and α -GaN{1 $\bar{1}03$ } reflections, the latter being tilted by 2.5° compared to the α -

GaN[1 $\bar{1}$ 00] substrate direction [see inset of Figure 5(d)]. The reduced tilt compared to the theoretical expectation of 3.3° is attributed to residual strain in the ScN and top GaN layers. The asymmetry of the β -GaN(220) peak results from the superposition with the underlying ScN(220) reflection being nearly lattice-matched.

Our results indicate that thin III_A-nitrides like GaN, AlN and InN can be kinetically stabilized in their metastable β phase on ScN(110), thus enabling new metal-semiconductor heterostructures. However, the formation of wurtzite inclusions, a common problem during the growth of cubic III_A-nitrides, should be prohibited by using specific growth conditions as previously documented for growth on Si(001),³⁹ GaAs(001),⁴⁰ 3C-SiC.⁴¹ For instance, stabilizing a smooth β -GaN(110) surface using surfactants⁴² could be decisive to prevent the formation of {111} _{β -GaN} facets where α -GaN inclusions nucleate. On the other hand, new twin-free TMN heterostructures containing *e.g.* ScN, HfN and ZrN are suitable to be grown on our ScN/GaN(1 $\bar{1}$ 00) platform, since TMNs are thermodynamically stable in the cubic rock-salt phase.

In conclusion, we have studied the growth of GaN/ScN heterostructures on the low-symmetry GaN(1 $\bar{1}$ 00) surface, both on NW sidewalls and on free-standing substrates. Twin-free ScN(110) layers are obtained using this approach due to a specific epitaxial relationship for which the interface symmetries match the one of bulk ScN(110). The uniaxial epitaxial strain imposed by the substrate along the GaN[0001] direction plastically relaxes within the first MLs, leaving a residual strain of \approx 0.7% for ScN layers up to a thickness of 40 nm. Subsequent deposition of GaN on ScN/GaN(1 $\bar{1}$ 00) results in a kinetic stabilization of β -GaN that rapidly transforms into a twinned α -GaN layer nucleating on {111} _{β -GaN} facets. As a result, the epitaxial relationship for α -GaN on ScN drastically differs from the one of ScN on α -GaN. Importantly, our ScN/GaN(1 $\bar{1}$ 00) platform provides a new route for the epitaxy of twin-free heterostructures combining semiconductors and

metals like β -GaN, ScN, HfN and ZrN, which are all nearly lattice-matched.³

Methods

ScN shells between 3 and 100 nm thickness are grown in N-rich conditions by PAMBE on GaN NWs at 840 °C and with a substrate rotation speed of 2 – 3 rpm. Active N is provided by a plasma cell with an atomic flux of $1.5 \times 10^{15} \text{ s}^{-1} \text{ cm}^{-2}$, and Sc by a high-temperature effusion cell with an atomic flux of $1 - 2 \times 10^{14} \text{ s}^{-1} \text{ cm}^{-2}$. The N and Sc fluxes are calibrated by determining the growth rate of GaN and ScN layers grown in N-limited and Sc-limited regimes, respectively. The temperature is calibrated as described in Ref. 43. GaN NWs are grown via self-assembly on sputtered TiN films decorated with Si seeds.⁴⁴ This approach allows fabricating ensembles with a NW density below 10^9 cm^{-2} , which is useful to prevent shadowing between neighboring NWs during the shell growth.

ScN layers with a thickness between 25 and 40 nm are grown on free-standing $5 \times 10 \text{ mm}^2$ GaN(1 $\bar{1}$ 00) substrates at 740 °C with similar atomic fluxes as used for the NWs. A 100 nm thick GaN layer is deposited prior to the ScN to create smooth atomic steps.

GaN overgrowth on ScN is done at 740 °C, on NW shells with a III/V ratio of 0.4 and on ScN films in slightly Ga-rich conditions.

The orientation and lattice parameter of the growing films are monitored *in situ* by RHEED with an acceleration voltage of 20 kV and *ex situ* by XRD using a PANalytical X'Pert PRO MRD diffractometer. EBSD is carried out in a Zeiss Ultra-55 scanning electron microscope operated at 15 kV and equipped with an EDAX Hikari Super EBSD camera to identify different crystal phases and orientations. Last, the microstructure of dispersed NWs and of plan-view specimens (preparation described in Ref. 45) is characterized by TEM in a Jeol 2100F field emission microscope operated at 200 kV and equipped with a Gatan Ultra Scan 4000 charge coupled device. Diffraction patterns and HRTEM images are simulated using the JEMS software package, the latter by ap-

plying a multi-slice approach.

Acknowledgement The authors thank Anne-Kathrin Bluhm for SEM measurement, Doreen Steffen for TEM sample preparation and Carsten Stemmler for MBE maintenance. The authors are grateful to Michael Hanke for a critical reading of the manuscript. Funding from Deutsche Forschungsgemeinschaft and Agence Nationale de la Recherche through the project Nanoflex (ANR-21-CE09-0044) is gratefully acknowledged.

References

1. Jena, D.; Page, R.; Casamento, J.; Dang, P.; Singhal, J.; Zhang, Z.; Wright, J.; Khalsa, G.; Cho, Y.; Xing, H. G. The New Nitrides: Layered, Ferroelectric, Magnetic, Metallic and Superconducting Nitrides to Boost the GaN Photonics and Electronics Eco-System. *Jpn. J. Appl. Phys.* **2019**, *58*, SC0801.
2. Yan, R.; Khalsa, G.; Vishwanath, S.; Han, Y.; Wright, J.; Rouvimov, S.; Katzer, D. S.; Nepal, N.; Downey, B. P.; Muller, D. A.; Xing, H. G.; Meyer, D. J.; Jena, D. GaN/NbN Epitaxial Semiconductor/Superconductor Heterostructures. *Nature* **2018**, *555*, 183–189.
3. Saha, B.; Shakouri, A.; Sands, T. D. Rock-salt Nitride Metal/Semiconductor Superlattices: A New Class of Artificially Structured Materials. *Appl. Phys. Rev.* **2018**, *5*, 021101.
4. Fichtner, S.; Wolff, N.; Lofink, F.; Kienle, L.; Wagner, B. AlScN: A III-V Semiconductor Based Ferroelectric. *J. Appl. Phys.* **2019**, *125*, 114103.
5. Park, S. Y.; Jang, Y. J.; Youn, D. H. A Review of Transition Metal Nitride-Based Catalysts for Electrochemical Nitrogen Reduction to Ammonia. *Catalysts* **2023**, *13*.
6. Dastmalchi, B.; Tassin, P.; Koschny, T.; Soukoulis, C. M. A New Perspective on Plasmonics: Confinement and Propagation Length of Surface Plasmons for Different Materials and Geometries. *Adv. Opt. Mater.* **2016**, *4*, 177–184.
7. Gioti, M.; Arvanitidis, J.; Christofilos, D.; Chaudhuri, K.; Zorba, T.; Abadias, G.; Gall, D.; Shalaev, V. M.; Boltasseva, A.; Patsalas, P. Plasmonic and Phononic Properties of Epitaxial Conductive Transition Metal Nitrides. *J. Opt.* **2020**, *22*, 084001.
8. Grundmann, M. Formation of Epitaxial Domains: Unified Theory and Survey of Experimental Results. *Phys. Status Solidi B* **2011**, *248*, 805–824.
9. Viehland, D. D.; Salje, E. K. Domain Boundary-Dominated Systems: Adaptive Structures and Functional Twin Boundaries. *Adv. Phys.* **2014**, *63*, 267–326.
10. Wright, J.; Chang, C.; Waters, D.; Lüpke, F.; Feenstra, R.; Raymond, L.; Koscica, R.; Khalsa, G.; Muller, D.; Xing, H. G.; Jena, D. Unexplored MBE Growth Mode Reveals New Properties of Superconducting NbN. *Phys. Rev. Mater.* **2021**, *5*, 024802.
11. Largeau, L.; Dheeraj, D. L.; Tchernycheva, M.; Cirlin, G. E.; Harmand, J. C. Facet and In-Plane Crystallographic Orientations of GaN Nanowires Grown on Si(111). *Nanotechnology* **2008**, *19*, 155704.
12. Li, Q.; Westlake, K. R.; Crawford, M. H.; Lee, S. R.; Koleske, D. D.; Figiel, J. J.; Cross, K. C.; Fatholouloumi, S.; Mi, Z.; Wang, G. T. Optical Performance of Top-down Fabricated InGaN/GaN Nanorod Light Emitting Diode Arrays. *Opt. Express* **2011**, *19*, 25528.
13. Koester, R.; Hwang, J.-S.; Salomon, D.; Chen, X.; Bougerol, C.; Barnes, J.-P.; Dang, D. L. S.; Rigutti, L.; De Luna Bugallo, A.; Jacopin, G.; Tchernycheva, M.; Durand, C.; Eymery, J. M-Plane Core-Shell InGaN/GaN Multiple-Quantum-Wells on GaN Wires for Elec-

- roluminescent Devices. *Nano Lett.* **2011**, *11*, 4839–4845.
14. Pantle, F.; Karlinger, M.; Wörle, S.; Becker, F.; Höldrich, T.; Sirotti, E.; Kraut, M.; Stutzmann, M. Crystal Side Facet-Tuning of GaN Nanowires and Nanofins Grown by Molecular Beam Epitaxy. *J. Appl. Phys.* **2022**, *132*, 184304.
 15. Waltereit, P.; Brandt, O.; Trampert, A.; Grahn, H. T.; Menniger, J.; Ramsteiner, M.; Reiche, M.; Ploog, K. H. Nitride Semiconductors Free of Electrostatic Fields for Efficient White Light-Emitting Diodes. *Nature* **2000**, *406*, 865–868.
 16. Fernando-Saavedra, A.; Albert, S.; Bengoechea-Encabo, A.; Trampert, A.; Xie, M.; Sanchez-Garcia, M. A.; Calleja, E. Growth of Non-Polar m-Plane GaN Pseudo-Substrates by Molecular Beam Epitaxy. *J. Cryst. Growth* **2023**, *617*, 127272.
 17. Casamento, J.; Wright, J.; Chaudhuri, R.; Xing, H. G.; Jena, D. Molecular Beam Epitaxial Growth of Scandium Nitride on Hexagonal SiC, GaN, and AlN. *Appl. Phys. Lett.* **2019**, *115*, 172101.
 18. Acharya, S.; Chatterjee, A.; Bhatia, V.; Pillai, A. I. K.; Garbrecht, M.; Saha, B. Twinned Growth of ScN Thin Films on Lattice-Matched GaN Substrates. *Mater. Res. Bull.* **2021**, *143*, 111443.
 19. Smith, A. R.; AL-Britthen, H. A. H.; Ingram, D. C.; Gall, D. Molecular Beam Epitaxy Control of the Structural, Optical, and Electronic Properties of ScN(001). *J. Appl. Phys.* **2001**, *90*, 1809–1816.
 20. Dinh, D. V.; Peiris, F.; Lähnemann, J.; Brandt, O. Optical Properties of ScN Layers Grown on Al₂O₃(0001) by Plasma-Assisted Molecular Beam Epitaxy. *Appl. Phys. Lett.* **2023**, *123*, 112102.
 21. Höglund, C.; Alling, B.; Birch, J.; Beckers, M.; Persson, P. O. Å.; Baetz, C.; Czirány, Z.; Jensen, J.; Hultman, L. Effects of Volume Mismatch and Electronic Structure on the Decomposition of ScAlN and TiAlN Solid Solutions. *Phys. Rev. B* **2010**, *81*, 224101.
 22. Wu, Y.; Wu, W.; Zou, X.; Xu, L.; Li, J. Growth and Great UV Emission Improvement of Highly Crystalline Quality Core–Shell ZnO/MgO Nanowires. *Mater. Lett.* **2012**, *84*, 147–150.
 23. Bierwagen, O.; Rombach, J.; Speck, J. S. Faceting Control by the Stoichiometry Influence on the Surface Free Energy of Low-Index Bcc-In₂O₃ Surfaces. *J. Phys.: Condens. Matter* **2016**, *28*, 224006.
 24. Stampfl, C.; Asahi, R.; Freeman, A. J. Surface Properties of the Refractory Metal-Nitride Semiconductor ScN: Screened-exchange LDA-FLAPW Investigations. *Phys. Rev. B* **2002**, *65*, 161204.
 25. Takeuchi, N.; Ulloa, S. E. First-Principles Calculations of the Structural and Electronic Properties of the ScN(001) Surface. *Phys. Rev. B* **2002**, *65*, 235307.
 26. Marlo, M.; Milman, V. Density-Functional Study of Bulk and Surface Properties of Titanium Nitride Using Different Exchange-Correlation Functionals. *Phys. Rev. B* **2000**, *62*, 2899–2907.
 27. Moram, M. A.; Barber, Z. H.; Humphreys, C. J.; Joyce, T. B.; Chalker, P. R. Young’s Modulus, Poisson’s Ratio, and Residual Stress and Strain in (111)-Oriented Scandium Nitride Thin Films on Silicon. *J. Appl. Phys.* **2006**, *100*, 023514.
 28. Yokozeiki, S. Theoretical Interpretation of the Moiré Pattern. *Opt. Commun.* **1974**, *11*, 378–381.
 29. Whaley, G. J.; Cohen, P. I. Relaxation of Strained InGaAs during Molecular Beam Epitaxy. *Appl. Phys. Lett.* **1990**, *57*, 144–146.
 30. Trampert, A.; Tournié, E.; Ploog, K. H. Novel Plastic Strain-relaxation Mode in

- Highly Mismatched III-V Layers Induced by Two-dimensional Epitaxial Growth. *Appl. Phys. Lett.* **1995**, *66*, 2265–2267.
31. Jallipalli, A.; Balakrishnan, G.; Huang, S.; Khoshakhlagh, A.; Dawson, L.; Huffaker, D. Atomistic Modeling of Strain Distribution in Self-Assembled Interfacial Misfit Dislocation (IMF) Arrays in Highly Mismatched III–V Semiconductor Materials. *J. Cryst. Growth* **2007**, *303*, 449–455.
 32. Jallipalli, A.; Balakrishnan, G.; Huang, S.H.; Rotter, T.J.; Nunna, K.; Liang, B.L.; Dawson, L.R.; Huffaker, D.L. Structural Analysis of Highly Relaxed GaSb Grown on GaAs Substrates with Periodic Interfacial Array of 90° Misfit Dislocations. *Nanoscale Res. Lett.* **2009**, *4*, 1458.
 33. Coraux, J.; Favre-Nicolin, V.; Renevier, H.; Proietti, M. G.; Amstatt, B.; Bellet-Amalric, E.; Daudin, B. Quantitative Structural Characterization of GaN Quantum Dot Ripening Using Reflection High-Energy Electron Diffraction. *J. Appl. Phys.* **2007**, *101*, 056106.
 34. Moram, M. A.; Vickers, M. E. X-Ray Diffraction of III-nitrides. *Rep. Prog. Phys.* **2009**, *72*, 036502.
 35. Trampert, A.; Brandt, O.; Yang, H.; Ploog, K. H. Direct Observation of the Initial Nucleation and Epitaxial Growth of Metastable Cubic GaN on (001) GaAs. *Appl. Phys. Lett.* **1997**, *70*, 583–585.
 36. Meyer, K.; Buchholz, M.; Schaadt, D. M. GaN Growth on (0 0 1) and (1 1 0) MgO under Different Ga/N Ratios by MBE. *J. Cryst. Growth* **2022**, *589*, 126681.
 37. Saengkaew, P.; Sanorpim, S.; Yordsri, V.; Thanachayanont, C.; Onabe, K. Characterization of Semi-Polar GaN on GaAs Substrates. *J. Cryst. Growth* **2015**, *411*, 76–80.
 38. Daldoul, I.; Othmani, S.; Mballo, A.; Vuong, P.; Salvestrini, J.; Chaaben, N. Growth and Characterization of Cubic GaN Grown on GaAs (110) Substrate by MOVPE. *Materials Science in Semiconductor Processing* **2021**, *132*, 105909.
 39. Nishimura, S.; Terashima, K. Growth of C-GaN on Si(100). *Mater. Sci. Eng. B* **2001**, *82*, 25–26.
 40. Yang, H.; Brandt, O.; Ploog, K. MBE Growth of Cubic GaN on GaAs Substrates. *Phys. Status Solidi B* **1996**, *194*, 109–120.
 41. Zscherp, M. F.; Mengel, N.; Hofmann, D. M.; Lider, V.; Ojaghi Dogahe, B.; Becker, C.; Beyer, A.; Volz, K.; Schörmann, J.; Chatterjee, S. AlN Buffer Enhances the Layer Quality of MBE-Grown Cubic GaN on 3C-SiC. *Cryst. Growth Des.* **2022**, *22*, 6786–6791.
 42. Mula, G.; Daudin, B.; Adelman, C.; Peyla, P. MBE Growth Of GaN Films In Presence Of Surfactants: The Effect Of Mg And Si. *MRS Internet J. Nitride Semicond. Res.* **2000**, *5*, 202–208.
 43. John, P.; Gómez Ruiz, M.; van Deurzen, L.; Lähnemann, J.; Trampert, A.; Geelhaar, L.; Brandt, O.; Auzelle, T. Growth Kinetics and Substrate Stability during High-Temperature Molecular Beam Epitaxy of AlN Nanowires. *Nanotechnology* **2023**, *34*, 465605.
 44. Auzelle, T.; Oliva, M.; John, P.; Ramsteiner, M.; Geelhaar, L.; Brandt, O. Density Control of GaN Nanowires at the Wafer Scale Using Self-Assembled SiNx Patches on Sputtered TiN(111). *Nanotechnology* **2023**, *34*, 375602.
 45. Luna, E.; Grandal, J.; Gallardo, E.; Calleja, J. M.; Sánchez-García, M. Á.; Calleja, E.; Trampert, A. Investigation of III–V Nanowires by Plan-View Transmission Electron Microscopy: InN Case Study. *Microsc. Microanal.* **2014**, *20*, 1471–1478.

Supporting Information:

ScN/GaN($1\bar{1}00$): a new platform for the epitaxy of twin-free metal-semiconductor heterostructures

P. John,* A. Trampert, D.-V. Dinh, D. Spallek, J. Lähnemann, V. Kaganer, L. Geelhaar, O. Brandt, and T. Auzelle

*Paul-Drude-Institut für Festkörperelektronik, Leibniz-Institut im Forschungsverbund Berlin e.V.,
Hausvogteiplatz 5-7, 10117 Berlin*

E-mail: john@pdi-berlin.de

The common orientation of epitaxial ScN on C-plane GaN, as also observed in this work for ScN grown on GaN nanowire top facets, is described by $\text{ScN}(111)[1\bar{1}0]||\text{GaN}(0001)[11\bar{2}0]$. The corresponding GaN(0001) and ScN(111) unit meshes, schematized in plan-view in Figure S1(a), exhibit the same atomic arrangement and quasi identical lattice parameters. The superposition of these planes thus results in a commensurate interface with negligible epitaxial strain. Nevertheless, twinning is inevitable due to the different GaN(0001) and ScN(111) rotational symmetries (6-fold and 3-fold, respectively), which are defined by the stacking of the subsequent monolayers not visible in the unit meshes.

If the same orientation was kept for ScN grown on the GaN($1\bar{1}00$) surface, the corresponding orientation-relationship would be described by $\text{ScN}(11\bar{2})[1\bar{1}0]||\text{GaN}(1\bar{1}00)[11\bar{2}0]$, leading to a hypothetical interface as schematized in Figure S1(b) in cross-sectional view. Although the inter-planar lattice distances along the GaN[0001] and ScN[111] directions match, the mismatch in AB_{GaN} and ABC_{ScN} stacking sequence leads to different lattice parameters. Epitaxy in this orientation would result in different bond lengths and angles between the atoms of both materials, thus preventing a simple atomic configuration at the interface and likely leading to a high density

of dangling bonds. Indeed, the dimensions of the corresponding GaN($1\bar{1}00$) and ScN($11\bar{2}$) plan-view unit meshes shown in Figure S1(c) show an enormous mismatch ($> 50\%$) along the GaN[0001] and ScN[111] directions. The superposition of these planes does not lead to a reasonable interface, making a ScN($11\bar{2}$) orientation on GaN($1\bar{1}00$) unlikely.

Instead, the epitaxial relationship experimentally observed in this work is given by $\text{ScN}(110)[001]||\text{GaN}(1\bar{1}00)[0001]$, as explained in the main manuscript and reproduced in Figure S1(d). Although this orientation involves a 13.1% uniaxial lattice mismatch, the fast strain relaxation via the coincidence site lattice including a periodic array of misfit dislocations (see main manuscript) seems to lead to an energetically more favorable interface.

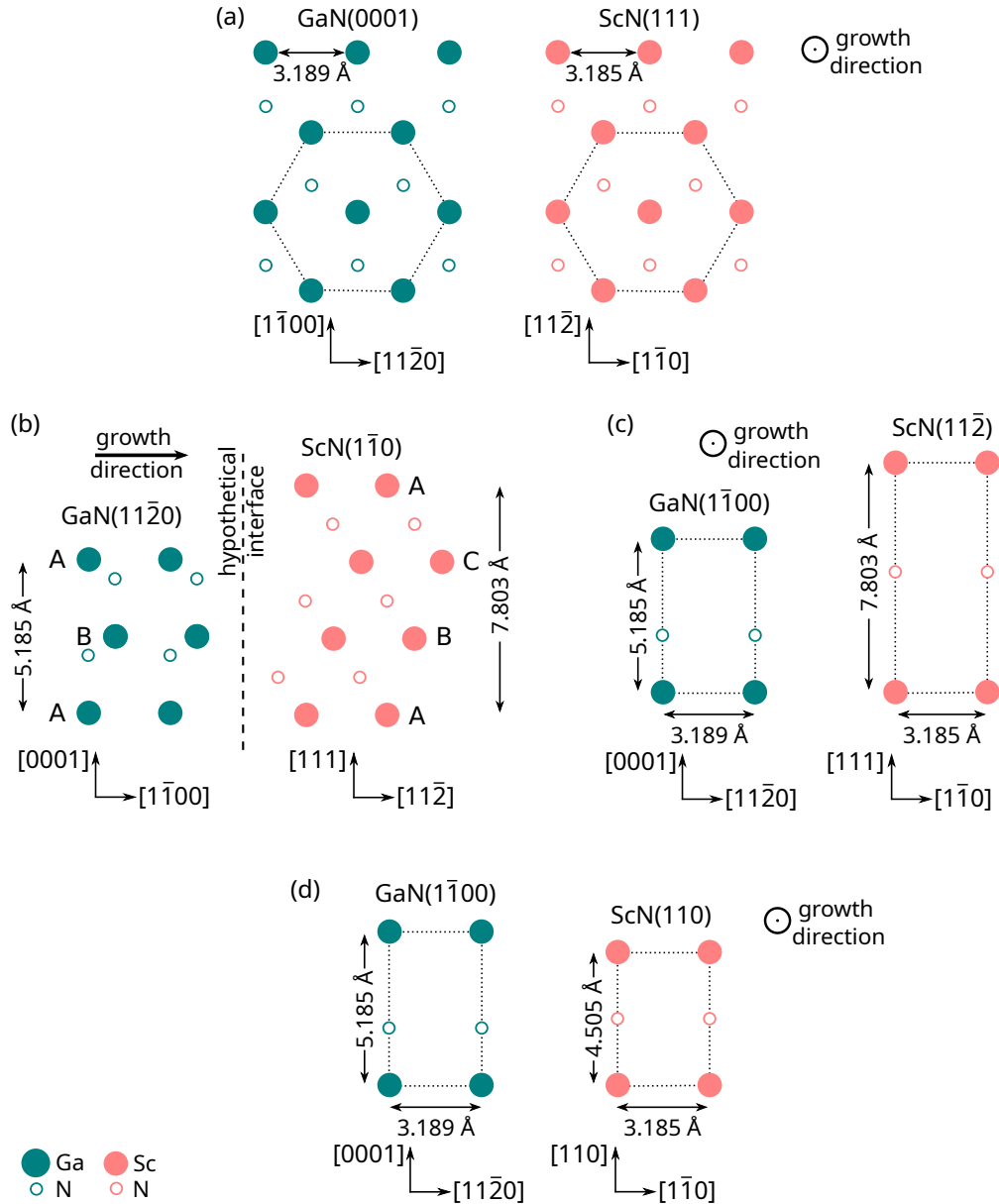


Figure S1: (a) Schematic two-dimensional GaN(0001) and ScN(111) unit meshes. (b) Schematic atomic arrangement of a hypothetical GaN(1100)/ScN(112) interface (in cross-sectional view), where (c) shows the corresponding GaN(1100) and ScN(112) plan-view unit meshes, which would need to be superimposed to keep the epitaxial relationship that is found for ScN on GaN(0001). (d) Two-dimensional GaN(1100) and ScN(110) unit meshes, showing the actual epitaxial relationship obtained in this work.